Journal of Medical Robotics Research

http://www.worldscientific.com/worldscinet/jmrr

Journal of Medical Robotics Research

Laser Incision Depth Control in Robot-Assisted Soft Tissue Microsurgery

Alperen Acemoglu[*,¶], Loris Fichera[*,‡], Ibolya E. Kepiro[†,§],
Darwin G. Caldwell[*], Leonardo S. Mattos[*]

[*]*Department of Advanced Robotics, Istituto Italiano di Tecnologia, Via Morego, 30, Genoa, 16163, Italy*

[†]*Nanoscopy & Nanobiophotonics, Department of Nanophysics*
Istituto Italiano di Tecnologia, Via Morego, 30, Genoa, 16163, Italy

[‡]*Department of Mechanical Engineering, Vanderbilt University*
2301 Vanderbilt Place, PMB 351592, Nashville, TN 37235, United States

[§]*National Physical Laboratory (NPL), Hampton Rd, Teddington, Middlesex, TW11 0LW, United Kingdom*
and
Faculty of Science, Engineering and Computing, Kingston University
Penrhyn Rd, Kingston-upon-Thames, London, KT2 1EE, United Kingdom

This paper presents the concept of a technology for the automation of laser incisions on soft tissue, especially for application in Transoral Laser Microsurgery (TLM) interventions. The technology aims at automatically controlling laser incisions based on high-level commands from the surgeon, i.e. desired incision shape, length and depth. It is based on a recently developed robotic laser microsurgery platform, which offers the controlled motion of the laser beam on the surgical site. A feed-forward controller provides (i) commands to the robotic laser aiming system and (ii) regulates the parameters of the laser source to achieve the desired results. The controller for the incision depth is extracted from experimental data. The required energy density and the number of passes are calculated to reach the targeted depth. Experimental results demonstrate that targeted depths can be achieved with $\pm 100\,\mu$m accuracy, which proves the feasibility of this approach. The proposed technology has the potential to facilitate the surgeon's control over laser incisions.

Keywords: Laser microsurgery; robotic surgery; incision depth; soft tissue; laser dosimetry.

JMRR

1. Introduction

The development of the CO_2 laser in 1964 [1] brought an alternative approach to perform incisions on soft tissues. In 1972, Jako *et al.* conducted animal studies to demonstrate the viability of performing surgical interventions in the larynx using a CO_2 laser as a tissue cutting

tool [2]. Three years later, Strong [3] reported on the use of a CO_2 laser in conjuction to a microscope for the excision of a laryngeal carcinoma from a human patient.

Laser surgery presents numerous advantages over traditional cold-steel surgery. These advantages include better control over bleeding, enhanced sterility of the surgical site, and the absence of post-operative edema [4,5]. Laser surgery is now an established alternative to radiation therapy for the treatment of laryngeal cancers [6,7]. A review by Milford and O'Flynn from 1991 provides a detailed comparitive study on radiotherapy and laser excision for the treatment of laryngeal carcinomas taking into account recurrence and total treatment period. The conclusion was a positive assessment of laser surgery as a valid alternative treatment [8]. Soon

after, it was reported that laser surgery enables effective treatment of T1 and T2 type tumors in the larynx, and constitutes a convenient and acceptable alternative for the patient [9].

Technological progress has transformed lasers in versatile tools for the treatment of diverse pathologies affecting delicate human organs. Together with other important applications such as eye surgery, transoral surgery is a major application field for lasers. Transoral Laser Microsurgery (TLM) is an evolution of the early techniques for laser surgery of the larynx. It includes a suite of minimally invasive endoscopic techniques for the excision of minuscule laryngeal diseases [7]. In degenerative diseases associated with cancer, the primary objective of TLM is to ensure a complete eradication of the malignant tissue. At the same time, surgeons try to minimize the removal of healthy tissues, to preserve as much organ function as possible [10]. The execution of such accurate resections requires the use of a microscope and precise control of the laser incisions.

In today's surgical practice, laser incisions are performed manually, i.e. moving a free-beam laser by means of a joystick-like device, called laser micromanipulator [7]. The micromanipulator is coupled to the operating microscope, forming an effective surgical device — yet, it is difficult to master, especially because it breaks the hand-eye coordination of the surgeon [11]. In addition, presently available technologies for TLM do not include any support for sensing the depth of laser cuts. The quality of incisions relies entirely on the dexterity and visual perception of clinicians. Extensive training is required to develop an effective laser cutting technique, which includes both (i) the acquisition of basic knowledge of the physical principles behind laser ablation of tissue; and (ii) the ability to manipulate the laser parameters and its exposure time in order to provide accurate cutting [7,10]. Parameters traditionally used in TLM include power, energy delivery mode, pulse duration and incision scanning frequency. The resulting incision depends on the combination of these parameters plus the total time of laser exposure. However, it is not evident how to regulate these parameters in order to achieve the desired cutting level. While experienced clinicians normally have sufficient knowledge and understanding of the laser ablation processes, lack of experience represents a practical problem for many others.

The limitation in terms of laser beam and surgical tools controllability in transoral surgeries has recently stimulated new research and technological developments towards robot-assisted systems for these procedures. For example, the da Vinci robot (Intuitive Surgical Inc., USA) has been used and is currently certified for operations in the mouth and throat. Studies have shown that the system brings many advantages to the procedures, including tremor filtering and increased dexterity through its articulated instruments [12]. However, the

use of this robot is limited by its large dimensions, long setup time, and high costs for the patient. Some of these limitations have been eliminated by flexible robotic systems developed specially for transoral surgeries, such as the Flex robot [13] and the RoboELF, a robotized endoscope for laryngeal surgery [14]. All of these systems can be used with fiber-coupled lasers, allowing enhanced controllability and access to laser-based surgeries. Nevertheless, the control of the laser dosimetry parameters is still performed by the surgeons without any assistance.

One important current limitation of fiber-based lasers for surgery is their poor focus control and requirement to work on contact with tissue to produce incisions. This translates into poor quality incisions with higher levels of thermal damage to surrounding healthy tissue when compared to free-beam surgery. Consequently, the use of free-beam surgical lasers is still preferred for delicate operations such as vocal cord surgery, and robot-assisted systems have been created specifically for these procedures [11,15,16]. Such technologies enable clinicians to control the laser position on the tissue through a teleoperated robotic device that replaces the traditional micromanipulator. Support is provided for motion scaling and tremor filtering, enabling more precise laser positioning. The control of laser aiming is further facilitated by the availability of user-defined motion patterns, which can be performed automatically by the system. A natural extension of these technologies is the automation of the laser incision process, based on high-level commands imparted by the surgeon.

Modeling laser tissue interactions for automated laser ablations in hard [17–20] and soft [21,22] tissue has been a field of interest in recent years. Controlled laser ablations on bone tissue with preplanned trajectories were performed using a robotic arm with 0.5 mm positioning error [17]. In another study, a simulation of the hard tissue ablation was developed to plan and predict the volume of the ablated tissue [18]. Moreover, incision depth was controlled intra-operatively using the inline coherent imaging which enables to measure current depth and terminate incision to achieve required depth [19]. Stopp *et al.* investigated the relation between laser energy, speed of laser motion and resulting ablation depth and compared their experimental results also to the theoretical model [20]. Bay *et al.* reported that real-time incision depth control on soft tissues can be achieved with the detection of shock waves collected from multiple acoustic detectors [21]. More recently, research performed by our research group established that the depth of a laser incision on soft tissue can be controlled regulating the exposure time of the laser [22]. The approach assumes a fixed laser motion pattern, i.e. repeated laser scans along a straight trajectory, at constant scanning frequency. Its applicability to different incision patterns (e.g. curved lines) and for different values of laser speed is yet to be explored. As a first

step in this direction, here we report on a study aim to model how the laser motion influences the resulting incision depth.

The effects of diode lasers on the width and depth of incisions on oral soft tissue have been studied and reported by Goharkhay *et al.* [23]. These experiments were based on a fixed speed of motion of the laser and concluded that the produced incision depth is only a dependent paramater of the average power of the laser [23]. In another study, researchers compared the effects of a 805 nm diode laser and a 1064 nm NdYag laser on soft tissue measuring the depths and the thermal damage of the incisions [24]. These studies provided a detailed overview on histological examinations, but the analysis of laser-tissue interactions were limited to the establishment of the clinical applicability of the lasers being tested. The analysis of the correlation between the laser parameters and their effects on soft tissue, including the laser scanning speed, the number of passes and the energy density, is still a remaining task to investigate. Building up a model with these physical quantities is essential for the development of an effective robot-assisted system for laser microsurgery.

Here, the concept of a technology for the automation of the laser incision process during TLM is presented. The idea is to create a controller capable of commanding a robotic device to automatically perform incisions of given depth, based on inputs provided by the surgeon. The objective is to overcome the difficulties associated with the manual regulation of the laser parameters, enabling a more intuitive user control on the laser incision depth. A theoretical model is derived, whose validity is assessed through controlled laser experiments which are performed to understand the effects of the parameters on incision depth.

2. Background

The automation of the laser incision process is based on a recently developed system for laser-based microsurgery, called the "μRALP Surgical System" [11]. As explained later in this section, the technology we propose constitutes an add-on component of this system. The μRALP system (Fig. 1(a)) is inspired by the current setup of TLM, of which it represents a revised, computer-assisted version. Here, the traditional micromanipulator is replaced by a graphics tablet, which enables a more intuitive (writing-like) control of the laser position. The commands imparted by the surgeon through this device are mapped into corresponding laser beam trajectories on the surgical site. The controlled motion of the laser is provided by a microrobotic system, based on a fast steering mirror [16]. The microscope is replaced by a stereoscopic head-mount display (HMD), which presents a magnified, 3D visualization of the surgical site.

This interface enables the intra-operative planning of laser trajectories that, once approved, are automatically executed by the system. Plans are defined and previewed in the HMD, through the superimposition of virtual overlays.

We propose to endow the μRALP system with the capability of automatically performing incisions based on high level surgeon inputs, i.e. incision length, shape and depth. To this end, a new user control is added to the surgeon interface, as shown in Fig. 1(b). This is a virtual control element, i.e. a graduated scale-bar that allows the surgeon to select the desired incision depth. With this new interface, the surgeon can pre-plan the incisions he wants to perform: the incision length and shape are defined using the graphics tablet, while the incision depth is regulated through the new virtual control element.
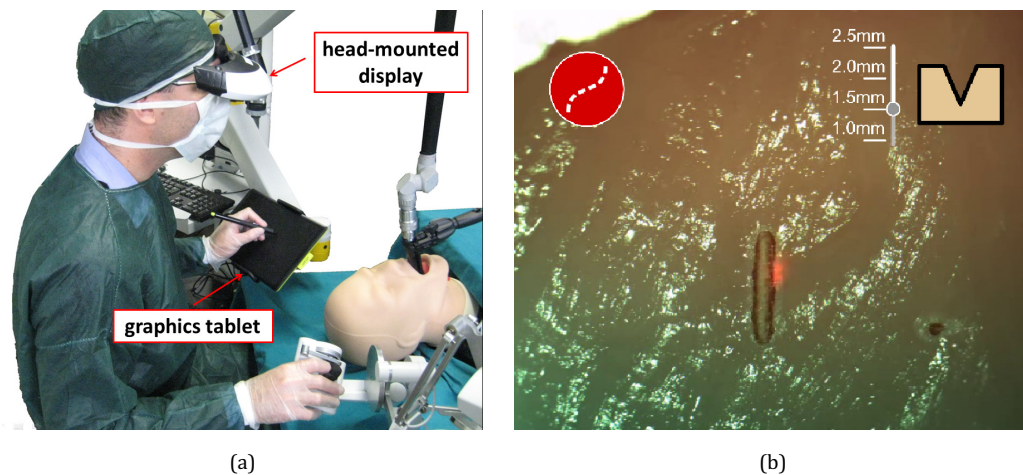

(a)　　　　　　　　　　　　　　(b)

Fig. 1. (a) The μRALP surgical interface. The surgeon visualizes the surgical site through a stereoscopic display (HMD) while controlling the position of the laser beam using a stylus and graphics tablet. (b) Technology concept. A virtual control element is superimposed to the surgeon interface, enabling an intuitive control of the laser incision depth.

The technology we propose relies on the availability of a controller capable of mapping the desired incision depth to appropriate laser parameters and activation. We have recently explored how the automatic activation/deactivation of the laser can be utilized to realize such a control [22]. The method uses a feed-forward controller based on a laser–tissue interaction model extracted from experimental data. Here we extend that work by incorporating the laser power and motion in the controller. A two-step approach is used: we first investigate the relation between the laser parameters and the theoretical spatial distribution of energy delivered to the tissue. Then, we study the relation between the spatial distribution of energy and the resulting laser incision depth.

Fig. 2. The motion of laser from point a to b can be represented as a curve $\gamma \in \mathbb{R}^2$.

3. Modeling the Laser Incision Process

In current surgical practice, incisions are produced by repeatedly moving the laser beam along desired cutting paths on the tissue. Laser scanning uses motorized mirrors to deflect the laser beam, enabling the automatic execution of preprogrammed cutting patterns. High-frequency cycles of the laser motion across the target tissue remove overlying layers with each pass.

CO_2 laser sources used in TLM present an emission in the infrared range (wavelength: $10.6\,\mu$m), which is strongly absorbed by the water content of the tissue [25]. This induces a thermal interaction that results in the vaporization of tissue. Ablation by vaporization is the fundamental physical process that enables the creation of surgical laser incisions. The resulting ablation crater presents the same shape of the laser beam [18].

3.1. *Spatial energy distribution*

Let us consider a small piece of tissue exposed to a laser beam. For the sake of simplicity, we assume the surface of the tissue to be flat. We further assume that the laser is firing uninterruptedly on the tissue, i.e. it is operating in continuous wave (CW) mode. A movement of the laser on the surface can be described as a curved area γ in $\mathbb{R}^2$, with endpoints a and b (see Fig. 2). From a fundamental physical law, considering ds is an infinitesimal increment along γ and dr an infinitesimal increment along the laser beam cross-section profile, each infinitesimal area $dA = ds \cdot dr$ receives an energy dose equal to the laser output power P times the duration of laser exposure:

$$\partial E = P\,\partial t, \tag{1}$$

where $E(J)$ is the total amount of energy delivered by the laser during its motion along γ. Equation (1) implies that the distribution of laser energy depends on the exposure time when using a constant power level (P): shorter exposure results in smaller delivered energy compared
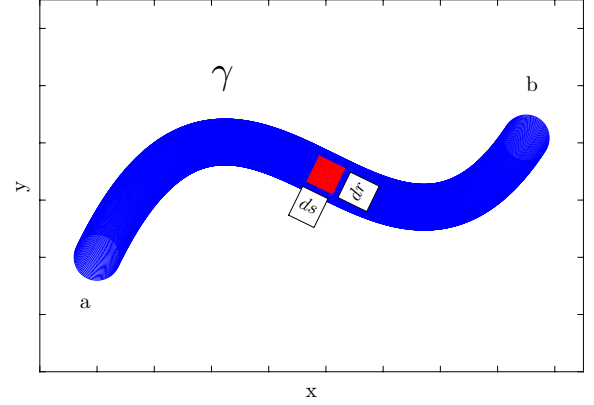
to longer exposures. This implies that the distribution of laser energy along the sweeping path depends on the speed of the laser motion: faster movements determine shorter exposures and, thus, smaller amount of energy; similarly, slower movements results in higher amounts of energy. We now define the energy density $e(A)$ (J/m^2) as the derivative of the energy E along γ;

$$e(A) = \frac{\partial E}{\partial r \partial s}\,n, \tag{2}$$

where $n \in \mathbb{N}$ represents the number of repeated passes (laser scans) performed on the tissue. Replacing the term E from Eq. (1) in Eq. (2) yields,

$$e(A) = \frac{P}{\partial r}\,\frac{\partial t}{\partial s}\,n. \tag{3}$$

This equation establishes a relation between the energy density $e(A)$ and the speed of laser motion: these two quantities are inversely proportional, with nP being the proportionality factor. Such a relation can be used to control the distribution of energy along the incision path, through the regulation of the laser power, speed of motion, and number of passes.

It is assumed that the laser is perfectly focused on the target tissue, which provides a constant laser spot diameter, w. With this assumption Eq. (3) can be simplified to:

$$e(A) = \frac{P}{w}\,\frac{\partial t}{\partial s}\,n. \tag{4}$$

We now consider the relation between the laser energy density $e(A)$ and the resulting incision depth $d(A)$. Prior research conducted in our laboratory has shown that the latter increases linearly with the total time of laser exposure, all other parameters being fixed [22,27]. Based on these evidence, here we hypothesize that a similar relation exists between $e(A)$ and $d(A)$, i.e.

$$d(A) = \alpha \cdot e(A) + \beta, \tag{5}$$

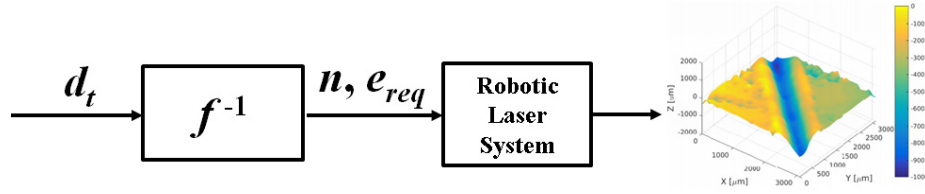where $\alpha, \beta \in \mathbb{R}^+$ in $\frac{\text{mm}^3}{\text{J}}$.

Fig. 3. The feed-forward controller scheme.

3.2. *Feed-forward controller*

In order to derive the feed-forward controller, the relation between energy density, e, the number of laser passes, n, and the incision depth, d, is investigated.

$$d = f(e, n). \tag{6}$$

Given the desired incision depth, d_t, our controller calculates the required number of passes, n, and required energy density, e_{req} (Fig. 3).

4. Methodology

4.1. *Experiments*

This section describes the experiments conducted to test the validity of the hypothesis formulated in the last section. Based on Eq. (4), $e(A)$ can be controlled through the manipulation of three distinct inputs, i.e. the laser power P, the speed of motion $\frac{\partial s}{\partial t}$, and the total number of laser passes n. It should be noted that the same energy density can be delivered to the tissue using different combinations of these three inputs. Therefore, we first investigate whether the depth of incision depends solely on the energy density, or the specific combination of laser inputs. Later on, we report on an experiment aimed at understanding the feasibility of controlling the laser incision depth automatically. In all experiments, it is assumed that laser spot is focused perfectly with $250\,\mu$m diameter ($w = 250\,\mu$m).

4.1.1. *Single-pass experiment*

We performed an experiment to compare the effects of creating the same energy distribution $e(A)$ through different combinations of laser power and speed. To exclude the effect of repeated laser passes on the resulting incision depth, single-pass incisions were performed, i.e. $n = 1$. The experimental design involves three pairs of conditions: for each pair, we fixed the amount of energy involved. The assigned values were $e(A) = [1.2, 2.4, 3.6]\,(\frac{J}{mm^2})$. These have been selected in order to cover the typical range of energy used during real laser microsurgeries. Each of these experimental conditions was implemented using two different combinations of laser power/speed. We performed three repetitions for each configuration, resulting in a total of 18 incision trials.

4.1.2. *Multiple pass experiment*

The focus of this experiment is on understanding the effect of repeated laser passes, performed at constant speed and with fixed laser power, on the resulting incision depth. To this aim, we performed a set of incision trials each time increasing number of passes, i.e. $n = [1, 2, 4, 6]$. The same set was repeated with two different combinations of laser power, i.e. $P = [4, 8]\,$W. Speed was set to $\frac{\partial s}{\partial t} = [13.33, 26.67]\,\frac{mm}{s}$, respectively. Each combination is repeated three times, resulting in a total of 24 incision trials.

4.1.3. *Computer-controlled laser incision trials*

The aim of this experiment is to understand the feasibility of creating specific target incision depths by controlling the energy density $e(A)$ created by the laser system. The relation between these two quantities is established through a regression method based on the data collected during the previous two experiments, as we shall see in the results section. Here we use the inverse of such relation to drive the selection of the number of laser passes and energy density required to realize the target depth.

The experiment involves three different target depths, i.e. $d = [0.3, 0.5, 0.8]\,$mm; for each target depth, we perform three repetitions, resulting in a total of nine trials. The laser power and speed are fixed to $P = 4\,$W and $\frac{\partial s}{\partial t} = [10.98, 10.12, 8.74]\,\frac{mm}{s}$, respectively. The selection of the number of laser passes n is performed using a procedure that limits the energy delivered in the course of a single pass. The motivation for using such an approach is that higher energy densities are known to induce stronger thermal interactions, thereby resulting in deformations of tissue that may hinder the repeatability of the trials. This effect was noticeable also in the results of the previous experiments, as will be shown later.

Algorithm 1: Laser dosimetry computation

1: d_{target} : Desired Incision Depth
2: e_{th} : Energy Density Threshold
3: P : Power
4: e_{req} : Required Energy Density
5: n : Number of Passes
6: **procedure**
7:     $n = 1$
8: top:
9:     Compute $e_{req} = f(d_{target})$
10:    **if** $(e_{req} > e_{th})$ **then**
11:       $n = n+1$
12:       $d_{target} = d_{target}/n$
13:       **goto** top.
14:    **else**
15:       Record n
16:       Record e_{req}
17:       Compute the $speed = f(e_{req}, P)$

The automatic procedure for computing the necessary number of laser passes and energy density to achieve a target incision depth is described as follows. First, the energy density $e(A)$ that would be required to reach the target depth using a single pass (i.e. $n = 1$) is computed. This is calculated based on laser–tissue interaction model learned for data gathered in the course of previous experiments. If the energy density value exceeds the threshold of $2 \frac{J}{mm^2}$, then the number of passes is incremented. This procedure is repeated until such condition is met. Algorithm 1 summarizes this laser dosimetry computation procedure.

The specific threshold value used was selected after analyzing the results from previous experiments, which indicated that energy densities smaller than this value result in more repeatable incision depth results. We performed three incisions for each configuration, resulting in a total of 9 incisions. For each incision, 20 measurements were performed as described later in Sec. 4.2.4.

4.2. *Materials and measurements*

In this section, we review the materials used in the experiments and measurement methods employed for the evaluation of the results.

4.2.1. *Laser source*

The experimental setup uses a commercial surgical laser source, a DEKA SmartXide^2 CO_2 (wavelength $10.6\,\mu m$, TEM_{00} beam profile). The HiScan Surgical laser scanner is used to regulate the speed of the laser spot on the tissue. Incision profile is a 5 mm straight line defined with the interface of the system in all experiments.

4.2.2. *Soft tissue samples*

Ex vivo chicken muscle tissue was used in these experiments. This type of soft tissue has a high water content, which makes it a suitable target for CO_2 laser ablation trials. Before the experiments, tissue samples were kept for 10 min in an open refrigerated box at a controlled temperature (7–12°C), in order to preserve their moisture and prevent degradation. To ensure identical initial temperature, the samples were monitored with an infrared thermal camera. Different tissue samples were used for each experimental condition, adding to the experiments a random effect. It is important to point out that the tissue model selected in this study may not present the same laser absorption profile that would be found in tissues *in vivo* conditions, since the thermal effects of a laser on living tissues are influenced by factors that are not present in *ex vivo* models [25], e.g. convective heat transfer due to blood perfusion. Nonetheless, most of these factors can be neglected in a first approximation [25] for the purpose of this proof-of-concept study. Indeed, chicken muscle tissue was selected and used for convenience since it is easily available and facilitates tissue manipulation, sample preparation and the incision depth measurements. Future research will focus on translating the modeling and control methods developed here to more realistic scenarios through trials to work out protocols on *ex vivo* pig larynxes and *in vivo* animal tissues.

4.2.3. *Microscope examination*

For estimating the parameters of the incision craters, confocal images (Leica SP5 microscope, Leica Microsystems GmbH, Germany) were analyzed. The resolution of the images had to be compromised so as to accommodate the dimension of the specimen using a HCX PL Fluotar 5×/0.15 numerical aperture (NA) WD 13.7 mm air objective. The images were acquired using an upright configuration in reflection mode with emission line centered at 488 nm. This optical configuration enables the analysis of area up to $3.1 \times 3.1\,mm^2$. Preliminary trials revealed that a lateral (XY) resolution of $6.06\,\mu m$ per pixel and an axial (Z) resolution of $30\,\mu m$ provide an adequate trade-off between the level of image detail and the acquisition time. The lateral and axial resolutions can be regulated by the user using objectives with different NA and laser lines.

Microscopic images have been processed with an extended depth of field algorithm [26], that produces a depth map representing the three-dimensional topology of the sample surface (see Fig. 4).

4.2.4. *Measurement of the incision depth*

An example of incision profile is shown in Fig. 5. We use a two-term Gaussian fitting procedure to approximate
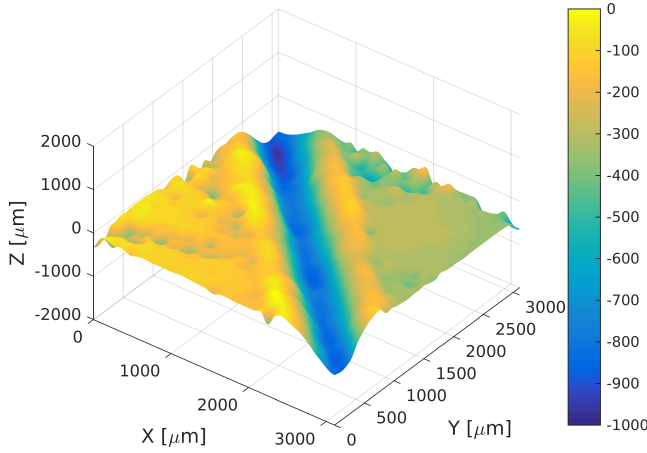
Fig. 4. Example of a depth map showing an incision crater produced on top of a tissue sample. This map has been reconstructed from microscopic images using the algorithm described by Aguet *et al.* [26]. Color-bar is in μm.
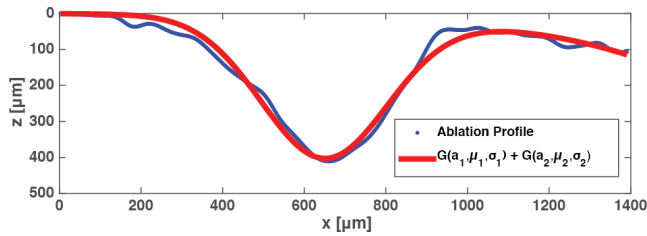

Fig. 5. Example of Gaussian fitting. Estimated parameters are amplitude (a), mean (μ), standard deviation (σ). For this particular example, $a_1 = 392.7$, $\mu_1 = 649.7$, $\sigma_1 = 219.1$, $a_2 = 2 \cdot 10^6$, $\mu_2 = 7649$, $\sigma_2 = 2000$. The parameter a_1 is taken as the depth of the crater.

the lateral profile of the incision. Boundaries are imposed on the fitting problem, so that (i) one-term models the altitude and profile of the tissue surface, while (ii) the second term models the profile of the ablation crater produced by the laser.

The amplitude of this latter term is taken as measure of the laser incision depth. The profile of each incision crater is sampled at intervals along its central part. Sampling interval is $60\,\mu$m, resulting in 20 profiles for each incision trial.

5. Results

5.1. *Single-pass experiment*

The plot in Fig. 6 summarizes the results for each of the six experimental configurations. The choice of a higher laser power level was found to produce deeper incisions, the energy density $e(A)$ being equal. We performed a Kruskal Wallis test to support that measurement results

for each pair of 4W and 8W are not overlapping; the results of the test show that the null hypothesis was rejected with the following *p*-values, $1.81e^{-9}$, $1.24e^{-12}$ and $3.39e^{-10}$ for 1.2, 2.4 and 3.6 $\frac{J}{mm^2}$, respectively. Table 1 reports the mean and spread (standard deviation) observed for each experimental configuration. The difference in the mean depth was found to increase for different power levels as the applied energy is increased (Fig. 6).

For each laser power value considered, the relation between the energy density and the incision depth was found to be linear, with a fitting root mean squared error (RMSE) of 2.11 μm for 4 W, and RMSE $= 27.13\,\mu$m for 8 W.
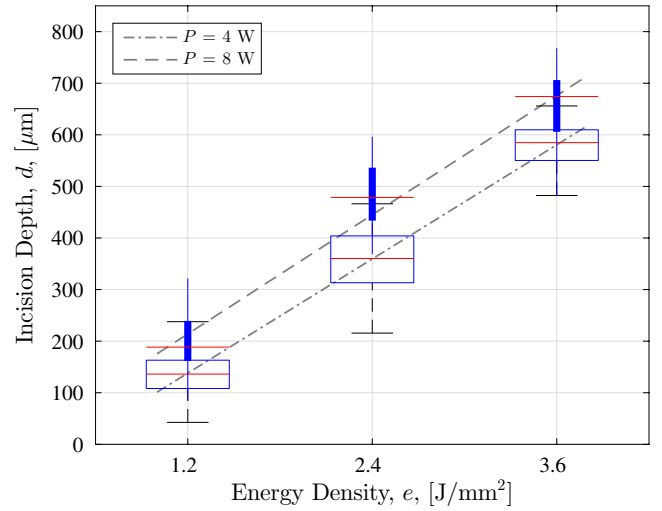

Fig. 6. Incision depth, d [μm], produced with different combination of laser power and speed in chicken muscle tissue (see Table 1). Results obtained with laser power $P = 4$ W are represented by *empty box plots*, while those for $P = 8$ W are represented by *filled box plots*. For a given value of laser power, the incision depth depends linearly on the energy density (for 4 W, $d = 181.2 \cdot e - 73.8$ and for 8 W, $d = 211.9 \cdot e - 48.7$).

Table 1. Variance of incision depth produced with different combinations of laser power and speed.

e(A) $\left(\frac{J}{mm^2}\right)$	Power (W)	Speed $\left(\frac{mm}{s}\right)$	Mean depth (μm)	Standard deviation (μm)
1.2	4	13.33	143	39.60
	8	26.67	194	52.97
2.4	4	6.67	362	57.85
	8	13.33	483	64.67
3.6	4	4.44	578	40.89
	8	8.89	703	67.82

Table 2. Results of the controlled incision trials

Target (μm)	n	e(A) ($\frac{J}{mm^2}$)	Speed ($\frac{mm}{s}$)	Mean depth (μm)	Standard deviation (μm)
300	2	1.457	10.98	286	69.66
500	3	1.582	10.12	471	54.66
800	4	1.830	8.74	761	47.28

5.2. Multi-pass experiment

The plots in Fig. 7 show the relative depth increment $\Delta d = d/\overline{d_s}$, where $\overline{d_s}$ is defined as the mean incision depth created with a single laser pass (i.e. $n = 1$). In the experimental scenario with laser power $P = 4\,\text{W}$, the mean values of Δd were 1.93, 3.96 and 5.47 for 2, 4 and 6 passes, respectively. A linear regression $\Delta d = \alpha n + \beta$

with parameters $\alpha = 0.91, \beta = 0.14$ approximates these points with RMSE = 0.13. A smaller increment rate was observed for $P = 8\,\text{W}$ ($\alpha = 0.76, \beta = 0.31$). The approximation error obtained in the scenario was higher with respect to the lower-power configuration, i.e. RMSE = 0.28. This can be largely attributed to the results obtained with higher number of passes ($n = [4, 6]$), that, as can be seen from Fig. 7(b), present a deviation from a linear behavior. Mean relative increments observed for this scenario are 1.66, 3.79 and 4.59 for 2, 4 and 6 passes, respectively.

5.3. Computer-controlled laser incisions

Computer-controlled laser incisions were performed considering the target depths presented in Table 2. For each case, the laser dosimetry parameters were
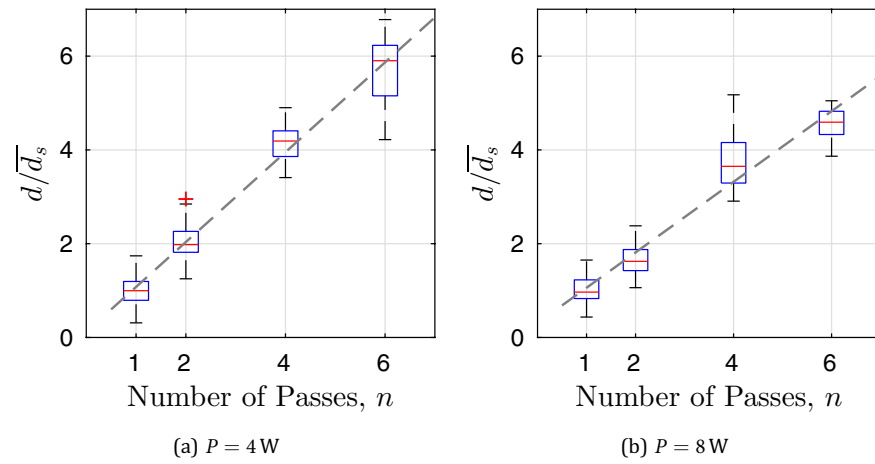

(a) $P = 4\,\text{W}$ (b) $P = 8\,\text{W}$

Fig. 7. Relative incision depth, $d/\overline{d_s}$ for different number of passes. $\overline{d_s}$ is average depth of the incisions produced with single pass. For all configurations, energy density, e, is fixed to $1.2\frac{J}{mm^2}$ and data are presented for $P = 4\text{W} - \overline{d_s} = 143\,\mu\text{m}$ (a), and $P = 8\,\text{W} - \overline{d_s} = 194\,\mu\text{m}$ (b).
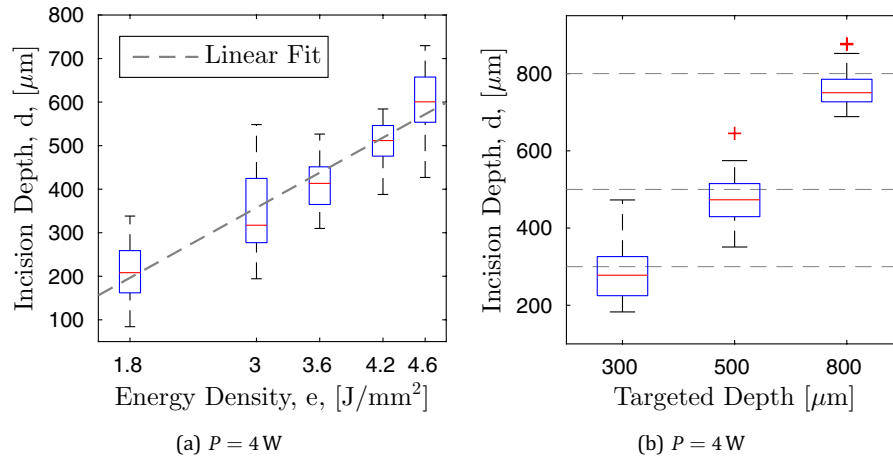

(a) $P = 4\,\text{W}$ (b) $P = 4\,\text{W}$

Fig. 8. (a) Incision depth, d [μm], for different energy densities, e [$\frac{J}{mm^2}$], and linear regression used to calculate the parameters for targeted depths. (b) Incision depth, d [μm], for targeted depths [μm].
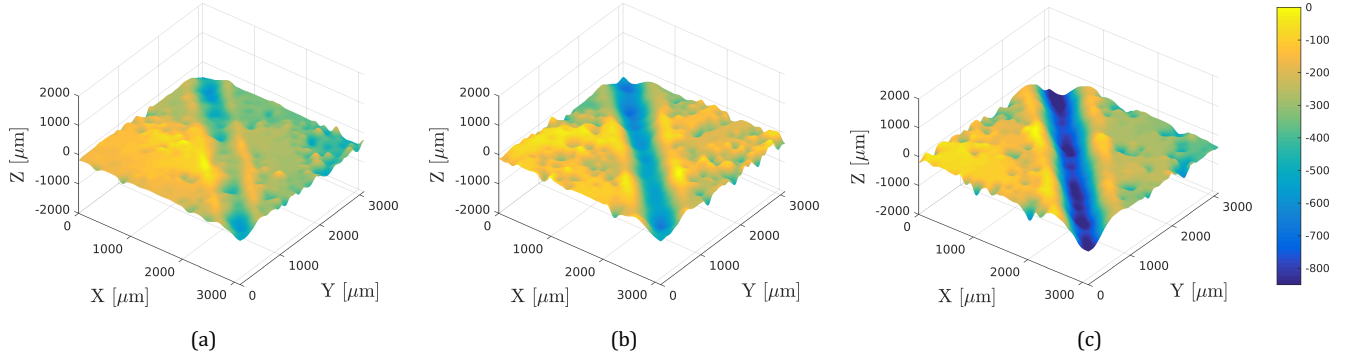
Fig. 9. Comparison of depth maps of incisions performed with different energy densities and number of passes for targeted values; (a) 300 μm, (b) 500 μm, (c) 800 μm. Color-bar is in μm.

computed using the linear regression model presented in Fig. 8(a) and Algorithm 1, which defined both the number of laser passes and the energy density values to be used to achieve the desired incision depths. The table also reports the mean and standard deviation for each experimental condition. The measured incision depths can be compared visually against their targets in Fig. 8(b). Deviations from the target are 4.67%, 5.8% and 4.87% for 300, 500 and 800 μm, respectively. Figure 9 shows a sample incision depth map for each of the three experimental conditions.

The residual error plot for computer-controlled incisions is depicted in Fig. 10. The results show that the residual errors are concentrated around zero with a tendency to negative values indicating that the incisions tended to be slightly shallower than the commanded values.
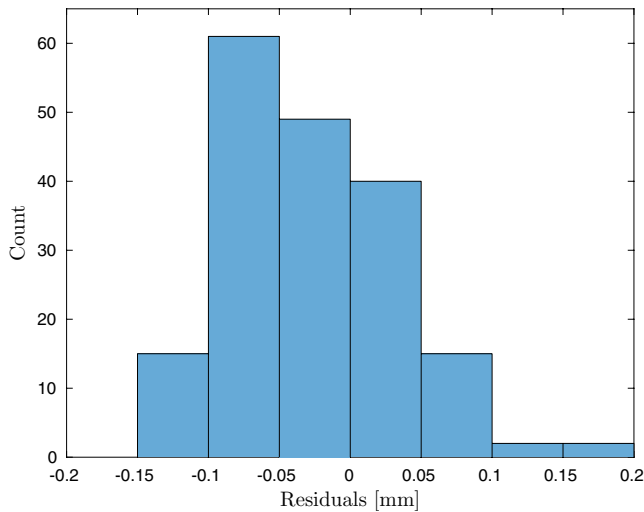

Fig. 10. Histogram plot showing residual errors for the computer-controlled incision trials.

6. Discussion

Results of the single-pass experiments indicate that knowledge of the laser energy density alone is not sufficient to predict the laser incision depth: the laser power must be also taken into account. In the literature, laser incision depth has been considered as a simple function of the total amount of energy delivered by laser [28]. However, results demonstrated that incision depth increases as the power is increased for the same energy density level.

The relation between incision depth and energy density is linear, when the power of the laser is fixed, as postulated in Eq. (5). This result is consistent with previous works [22,27] where the authors reported a linear relation between exposure time and incision depth.

Results of the multi-pass experiment present linear behavior for the relation between relative incision depth and number of passes. In addition to this, our multi-pass experiments results show that the deepest incisions are not more than 916 μm. In a previous study where researchers performed multi-pulse laser incision experiment on bone tissue [17], it has been reported that the number of pulse–depth relation is linear up to 1 mm depth whereas logarithmic relation exists up to 2 mm. As in that case, also here it has been observed that when incisions are performed with several passes, as the incision goes deeper, energy dissipation is observed due to changing focus of the laser spot, incision debris and increasing the surface area of incision [17].

Multi-pass experiment results for 4 W show that relative incision depths, Δd, for all data points are close to unity. Increasing the power to 8 W causes the relationship to deviate from being linear. In this set of experiments, incisions are performed with higher speed and higher power. A possible reason for deviation from linearity can be higher thermal deformations at high power levels. It is also reported that temperature increases start earlier at higher power [29]. Authors also

reported that instant temperature rises up to $20\,^{\circ}$C are observed for the incisions produced with 12 W. There is not sufficient time for thermal relaxation with the incisions in the CW mode in contrary to pulsed laser incisions. Thus, the remaining heat after vaporization of the tissue is dissipated to neighboring tissue, causing also the ablation of these structures when working at higher power levels [29].

For computer-controlled incisions, 4 W has been selected due to the low standard deviation in single-pass experiments and highly linear behavior in multi-pass experiments. Computer-controlled incision results indicate that targeted depth can be achieved within $\pm 100\,\mu$m error range. However, as Table 2 shows, mean depth errors were only 14, 29 and $39\,\mu$m for 300, 500 and $800\,\mu$m targeted depths, respectively. Highest mean error was observed for $800\,\mu$m targeted depth, which was performed with 4 passes, i.e. $n = 4$. As discussed earlier, as the number of passes increases in multi-pass incisions, the resulting incision depth tends to deviate from linear behavior due to the energy dissipation. Nevertheless, the measured standard deviations were significantly small: 69.66, 54.66 and $47.28\,\mu$m for 300, 500 and $800\,\mu$m, respectively. This indicates the proposed technology provides repeatable results.

7. Conclusion

In this paper, we presented the concept of a technology to automate laser incisions on soft tissue for laser microsurgery applications. An existing robotic laser device is used to realize the laser motion on the surgical site. A feed-forward controller maps high-level commands imparted by the surgeon to the laser parameters required to achieve the desired incisions. The controller is based on an inverse model, which is extracted from experimental data using regression techniques.

Experimental evidence presented here indicates that the depth of a laser incision can be regulated controlling the energy density along the incision path and number of passes with an accuracy of $\pm 100\,\mu$m. Our results provide data on the methodological concept for an extended protocol for the implementation and validation of an improved robot-assisted technology in real laser microsurgery conditions in clinical setting. However, a clinical implementation of this new technology will still require the use of the proposed method for the derivation of new models considering the same type of living tissues encountered during real laser microsurgeries. This is required because the properties of the living tissues, such as the water and blood content, vary not only between different tissue types, but also significantly from *ex vivo* conditions [30]. Therefore, in order to validate the proposed system and bring it closer to clinical application in the operating room, it is crucial to extend this work with

in vivo experiments. Enough data will have to be collected to create models that generalize well and allow good incision depth control by applying the same methodology presented here.

Given that at the present time no technology is available to control or supervise the creation of laser incisions during laser microsurgeries, the technology proposed in this paper represents a significant advancement to the state-of-the-art technology for laser microsurgery. It has the potential to facilitate and significantly enhance the surgeon's capacity to create precise laser incisions, allowing clinical reasoning based on more intuitive quantities — i.e. the incision depth — and leaving to the robotic system the task of regulating the energy delivered to achieve the desired results. In the future, we will also explore the integration of the haptic feedback into the models developed here. Our previous research demonstrated that introducing the haptic feedback into the laser microsurgery workflow allows significant improvements in performance in laser incision depth control [31].

References

1. C. K. N. Patel, Continuous-wave laser action on vibrational-rotational transitions of CO_2, *Phys. Rev.* **136**(5A) (1964) A1187.
2. G. J. Jako, Laser surgery of the vocal cordsan experimental study with carbon dioxide lasers on dogs, *The Laryngoscope* **82**(12) (1972) 2204–2216.
3. M. S. Strong, Laser excision of carcinoma of the larynx, *The Laryngoscope* **85**(8) (1975) 1286–1289.
4. C. W. Vaughan, M. S. Strong and G. J. Jako, Laryngeal carcinoma: Transoral treatment utilizing the CO 2 laser, *Am. J. Surg.* **136**(4) (1978) 490–493.
5. J. M. White, H. E. Goodis and C. L. Rose, Use of the pulsed Nd: YAG laser for intraoral soft tissue surgery, *Lasers Surg. Med.* **11**(5) (1991) 455–461.
6. E. M. Skolnik, L. Martin, K. F. Yee and M. A. Wheatley, Radiation failures in cancer of the larynx, *Ann. Otol. Rhinol. Laryngol.* **84**(6) (1975) 804–811.
7. M. Rubinstein and W. B. Armstrong, Transoral laser microsurgery for laryngeal cancer: A primer and review of laser dosimetry, *Lasers Med. Sci.* **26**(1) (2011) 113–124.
8. C. A. Milford and P. E. O'Flynn, Management of verrucous carcinoma of the larynx, *Clin. Otolaryngol. Allied Sci.* **16**(2) (1991) 160–162.

9. H. E. Eckel and W. F. Thumfart, Laser surgery for the treatment of larynx carcinomas: Indications, techniques, and preliminary results, *Ann. Otol. Rhinol. Laryngol.* **101**(2) (1992) 113–118.

10. W. Steiner and P. Ambrosch, *Endoscopic Laser Surgery of the Upper Aerodigestive Tract: With Special Emphasis on Cancer Surgery* (Thieme, 2000).

11. N. Deshpande, J. Ortiz, D. Caldwell and L. Mattos, Enhanced computer-assisted laser microsurgeries with a "virtual microscope" based surgical system, in *Proc. IEEE Int. Conf. Robotics and Automation (ICRA)* (2014), pp. 4194–4199.

12. N. G. Hockstein, J. P. Nolan, B. W. O'Malley and Y. J. Woo, Robotic microlaryngeal surgery: A technical feasibility study using the daVinci surgical robot and an airway mannequin, *The Laryngoscope* **115**(5) (2005) 780–785.

13. C. M. Rivera-Serrano, P. Johnson, B. Zubiate, R. Kuenzler, H. Choset, M. Zenati, S. Tully and U. Duvvuri, A transoral highly flexible robot, *The Laryngoscope* **122**(5) (2012) 1067–1071.

14. K. Olds, A. T. Hillel, E. Cha, M. Curry, L. M. Akst, R. H. Taylor and J. D. Richmon, Robotic endolaryngeal flexible (RoboELF) scope: A preclinical feasibility study, *The Laryngoscope* **121**(11) (2011) 2371–2374.

15. L. S. Mattos, N. Deshpande, G. Barresi, L. Guastini and G. Peretti, A novel computerized surgeonmachine interface for robot-assisted laser phonomicrosurgery, *The Laryngoscope* **124**(8) (2014) 1887–1894.

16. L. Mattos, G. Dagnino, G. Becattini, M. Dellepiane and D. Caldwell, A virtual scalpel system for computer-assisted laser microsurgery, *2011 IEEE/RSJ Int. Conf. Intelligent Robots and Systems* (2011), pp. 1359–1365.

17. J. Burgner, M. Müller, J. Raczkowsky and H. Wörn, Ex vivo accuracy evaluation for robot assisted laser bone ablation, *Int. J. Med. Robot. Comput. Assist. Surg.* **6**(4) (2010) 489–500.

18. L. A. Kahrs, J. Burgner, T. Klenzner, J. Raczkowsky, J. Schipper and H. Wörn, Planning and simulation of microsurgical laser bone ablation, *Int. J. Comput. Assist. Radiol. Surg.* **5**(2) (2010) 155–162.

19. B. Y. Leung, P. J. Webster, J. M. Fraser and V. X. Yang, Real-time guidance of thermal and ultrashort pulsed laser ablation in hard tissue using inline coherent imaging, *Lasers Surg. Med.* **44**(3) (2012) 249–256.

20. S. Stopp, D. Svejdar, E. von Kienlin, H. Deppe and T. C. Lueth, A new approach for creating defined geometries by navigated laser ablation based on volumetric 3-D data, *IEEE Trans. Biomed. Eng.* **55**(7) (2008) 1872–1880.

21. E. Bay, X. L. Deán-Ben, G. A. Pang, A. Douplik and D. Razansky, Real-time monitoring of incision profile during laser surgery using shock wave detection, *J. Biophoton.* **8**(1–2) (2015) 102–111.

22. L. Fichera, D. Pardo, P. Illiano, D. G. Caldwell and L. S. Mattos, Feed forward incision control for laser microsurgery of soft tissue, *2015 IEEE Int. Conf. Robotics and Automation (ICRA)* (2015), pp. 1235–1240.

23. K. Goharkhay, A. Moritz, P. Wilder-Smith, U. Schoop, W. Kluger, S. Jakolitsch and W. Sperr, Effects on oral soft tissue produced by a diode laser in vitro, *Lasers Surg. Med.* **25**(5) (1999) 401–406.

24. M. M. Judy, J. L. Matthews, B. L. Aronoff and D. F. Hults, Soft tissue studies with 805 nm diode laser radiation: Thermal effects with contact tips and comparison with effects of 1064 nm Nd: YAG laser radiation, *Lasers Surg. Med.* **13**(5) (1993) 528–536.

25. M. Niemz, *Laser-Tissue Interactions* (Springer Berlin Heidelberg, 2004).

26. F. Aguet, D. Van De Ville and M. Unser, Model-based 2.5-D deconvolution for extended depth of field in brightfield microscopy, *IEEE Trans. Image Process.* **17** (2008) 1144–1153.

27. L. Fichera, D. Pardo, P. Illiano, J. Ortiz, D. G. Caldwell and L. S. Mattos, Online estimation of laser incision depth for transoral microsurgery: Approach and preliminary evaluation, *Int. J. Med. Robot. Comput. Assist. Surg.* **12**(1) (2016) 53–61.

28. A. Vogel and V. Venugopalan, Mechanisms of pulsed laser ablation of biological tissues, *Chem. Rev.* **103**(2) (2003) 577–644.

29. P. Wilder-Smith, A. M. Arrastia, L. H. Liaw and M. Berns, Incision properties and thermal effects of three CO_2 lasers in soft tissue, *Oral Surg. Oral Med. Oral Pathol. Oral Radiol. Endodontol.* **79**(6) (1995) 685–691.

30. S. L. Jacques, Optical properties of biological tissues: A review, *Phys. Med. Biol.* **58**(11) (2013) p. R37.

31. L. Fichera, C. Pacchierotti, E. Olivieri, D. Prattichizzo and L. S. Mattos, Kinesthetic and vibrotactile haptic feedback improves the performance of laser microsurgery, *2016 IEEE Haptics Symp. (HAPTICS)* (2016), pp. 59–64.

Alperen Acemoglu received his B.Sc. degree in Mechanical Engineering from Istanbul Technical University, Turkey, in 2012, and M.Sc. degree in Mechatronics Engineering from Sabanci University, Turkey, in 2014. Now, he is a Ph.D. student in Biomedical Robotics Laboratory, Department of Advanced Robotics, Istituto Italiano di Tecnologia, Italy. His research interests include medical robotics, magnetic actuation, tendon-based micro-manipulators.

Loris Fichera received a B.Sc. (2008) and a M.Sc. (2011) in Computer Engineering from the University of Catania, and a Ph.D. from the Italian Institute of Technology (2015), where he conducted research with the Department of Advanced Robotics. He is currently a Postdoctoral Researcher with the Department of Mechanical Engineering, Vanderbilt University. His research interests include medical robotics and computer-assisted surgery, with a focus on image-guided interventions.

Ibolya E. Kepiro received an M.Sc. degree in biomedical physics and microscopy from the University of Szeged, Hungary in 2005 and worked as a postgraduate researcher and research scientist at the Department Ophthalmology until 2009. She completed a Ph.D. degree in high-resolution *in vivo* human retinal imaging at Imperial College London, UK in 2013. She was a postdoctoral research fellow at Nanoscopy & Nanobiophotonics, Italian Institute of Technology, Genova until 2015 where she worked on the Renvision EU FP7 project on *in vitro* high-resolution 3D structural mouse retinal imaging using light sheet- and confocal fluorescence microscopy. She is currently based at the National Physical Laboratory (NPL) London, UK. Her research interest includes nanoscopy and nanotechnology to solve challenging tasks in complex biological systems, immunohistochemistry, antimicrobial discovery, drug delivery, development of high-resolution imaging modalities for early diagnose and treatment of diseases, investigating intra- and extracellular matrices.

Darwin G. Caldwell is Deputy Scientific Director at the Italian Institute of Technology, Director of the Department of Advanced Robotics at IIT, and an Honorary Professor at the Universities of Sheffield, Bangor, Kings College London and Tianjin University China. His research interests include innovative actuators, humanoid and quadrupedal robotics (iCub, cCub, COMAN, WalkMan HyQ, and HyQ2Max), force augmentation exoskeletons, dexterous manipulators, and medical robotics. He is the author or co-author of over 500 academic papers, and 19 patents and has received awards from several international journals and conferences. In 2015 he was elected as a Fellow of the Royal Academy of Engineering.

Leonardo S. Mattos (B.Sc. 1998, M.Sc. 2003, Ph.D. 2007) is the Head of the Biomedical Robotics Laboratory, Department of Advanced Robotics, Istituto Italiano di Tecnologia. He was the PI and coordinator of the European project μRALP — Micro-Technologies and Systems for Robot-Assisted Laser Phonomicrosurgery. His research background includes micromanipulation, systems integration, development of user interfaces and systems for safe and efficient teleoperation, robotic surgery, computer vision, adaptive controllers and automation. Leonardo received his Ph.D. degree in electrical engineering from the North Carolina State University (NCSU, USA), where he worked as research assistant at the Center for Robotics and Intelligent Machines (CRIM) from 2002 until 2007. He has been a researcher at the IIT since 2007.